INSTITUTE OF PHYSICS PUBLISHING JOURNAL OF OPTICS A: PURE AND APPLIED OPTICS

J. Opt. A: Pure Appl. Opt. **6** (2004) 690–697 PII: S1464-4258(04)75616-0

Estimation of surface reflection effects on upwelling radiance field measurements in turbid waters

D Doxaran, R C Nagur Cherukuru and S J Lavender

School of Earth, Ocean and Environmental Sciences (SEOES), University of Plymouth, Drake Circus, Plymouth, Devon PL4 8AA, UK

E-mail: ddoxaran@plymouth.ac.uk

Received 30 January 2004, accepted for publication 28 April 2004
Published 11 June 2004
Online at stacks.iop.org/JOptA/6/690
doi:10.1088/1464-4258/6/7/006

Abstract

The contribution of surface reflection effects to above-water upwelling radiance measurements has been estimated from field optical data recorded in turbid coastal and estuarine waters. The water-leaving radiance signal was determined from underwater measurements and compared to the total upwelling radiance signal measured above the water surface with the sensor pointing towards the nadir, then adopting a recommended oblique viewing position. The observed differences are representative of surface reflection effects at the air/water interface (predominately sun and sky glint). These effects are analysed for different illumination conditions (cloud cover and solar zenith angle). Results are presented at four wavelengths representative of the visible and near-infrared spectral domains.

The contribution of surface reflection effects to above-water upwelling radiance measurements is highly variable and always significant (typically 50% in the visible and higher at short and near-infrared wavelengths). It is more stable (consistent value), but higher under diffuse light conditions.

The correction of surface reflection effects is problematic because the percentage of sky radiance reflected at the air/water interface (ρ) is unknown most of the time. An approximate correction (assuming a 0.02 ρ value) leads to large errors in the retrieved water-leaving signal. These errors are greatly minimized when considering a radiance ratio between two wavelengths.

Keywords: radiance, turbid waters, reflection effects, Tamar estuary

1. Introduction

The calibration and validation of ocean colour remote sensing data requires accurate field determinations of the water-leaving radiance signal (Mobley 1994). *In situ* above-water radiometric measurements are commonly used in turbid coastal waters (e.g. Froidefond *et al* 1991, 1999, Doxaran *et al* 2002a, 2002b, 2003) as underwater measurements are difficult due to the high attenuation. Such measurements are significantly influenced by surface reflection effects (predominately sun and sky glint) and must be accurately corrected if the signal backscattered by the water is to be retrieved. The recommended correction is the subtraction of a percentage of the sky radiance that is directly reflected at the air/water interface (Austin 1974, Mobley 1999), but it is highly dependent on the viewing geometry, illumination conditions and sea state (Fougnie *et al* 1999, Mobley 1999). Inaccurate corrections may result in significant uncertainties in the estimated water-leaving signal and errors when interpreting ocean colour remote sensing data.

The aim of this study was to estimate the respective contributions of the water-leaving signal and surface reflection effects to the above-water field radiometric measurements, in turbid coastal waters. The objective was to understand the significance of the surface reflection effects and their dependence on the viewing geometry and illumination

conditions, and thus assess the importance of accurate corrections.

Based on field optical data, the water-leaving radiance signal is determined from underwater measurements, unaffected by surface reflection effects. This signal is compared to above-water upwelling radiance measurements. The variations of the obtained differences are analysed as a function of the viewing geometry (position of the sensor above the water surface), illumination conditions (cloud cover and solar zenith angle) and water turbidity. The observations are discussed based on computational results obtained notably by Mobley (1999). A simple solution is proposed that would minimize these surface reflection effects.

2. Theoretical background

The optical signal commonly used in ocean colour remote sensing applications is the remote-sensing reflectance signal (R_{rs}, in sr^{-1}), defined as (Mobley 1994)

$$R_{rs} = \frac{L_w}{E_d(0^+)}, \quad (1)$$

where L_w (W m^{-2} sr^{-1} nm^{-1}) is the water-leaving radiance and $E_d(0^+)$ (W m^{-2} nm^{-1}) is the downwelling irradiance incident on the water surface. The wavelength dependence of the parameters is omitted to simplify the notation. L_w also depends on the viewing direction, defined by the zenith and azimuth angles θ_v and φ_v.

The calibration and validation of satellite and/or airborne ocean remote sensing data requires field R_{rs} measurements concurrently with the collection of water samples. $E_d(0^+)$ can be measured above the water surface, directly using an irradiance sensor, or using a radiance sensor and a reference (e.g. Spectralon) plaque of a known reflectance (Fargion and Mueller 2000). L_w cannot be directly measured and is determined from above-water or in-water measurements (Fargion and Mueller 2000).

In the first case, the total radiance signal (L_t) measured when pointing a sensor (radiometer) towards the water surface can be expressed as (Mobley 1999)

$$L_t = L_w + L_r, \quad (2)$$

where (L_r) is the radiance signal resulting from reflection effects at the air/water interface, namely the sun and sky glint. L_r is due to a certain percentage (ρ) of the sky radiance (L_{sky}) reflected at the surface (Austin 1974, Mobley 1999):

$$L_r = \rho L_{sky}. \quad (3)$$

ρ is a complex factor that depends on incident light and viewing directions, wavelength and wind speed. It is not an inherent optical property of the water surface as it also depends on the sensor field-of-view and sky radiance distribution. As indicated by Mobley (1999), ρ depends on, but does not equal, the Fresnel reflectance of the surface.

In the second case, L_w is determined from underwater upwelling radiance (L_u) measurements recorded along vertical profiles. In the water column, L_u is attenuated according to an exponential law (Fargion and Mueller 2000):

$$L_u(z) = L_u(0^-)\exp(-K_L z), \quad (4)$$

where z (in m) is the water depth, K_L (in m^{-1}) is the attenuation coefficient for radiance and $L_u(0^-)$ is the upwelling radiance just beneath the surface, at depth 0.

Then, L_w is determined from $L_u(0^-)$ by taking into account the refraction/reflection phenomena at the air/water interface (Morel and Gentili 1996, Mobley 1999):

$$L_w = \frac{1 - r_F}{n_w^2} L_u(0^-), \quad (5)$$

where n_w is the refractive index of water; r_F is the Fresnel reflectance (function of θ_v and its corresponding refracted angle in water θ'_v); $L_u(0^-)$ corresponds to the direction defined by the zenith and azimuth angles θ'_v and φ_v; θ'_v and θ_v are related according to Snell's law (refraction at water surface). Due to the low spectral variations of r_F and n_w, Morel (1980) and Austin (1980) propose the following approximation:

$$L_w(0^+) \approx 0.544 L_u(0^-). \quad (6)$$

3. Data and methods

3.1. Data

In June and August 2003, simultaneous water sample and field optical measurements were carried out in the UK Plymouth coastal waters that include the Tamar estuary (table 1). The transects on the 23/06, 24/06 and 05/08 were completed from Plymouth Sound to the upstream part of the Tamar estuary (corresponding to 12 and 13 stations, respectively). On the 26/06 and 27/06, the data (corresponding to 9 and 9 stations, respectively) were collected at a fixed station located in the upstream part of the Tamar estuary. Different illumination conditions were encountered during the fieldwork: clear, cloudy and covered skies (table 1). The sea surface was quasi-plane. Water samples were collected from surface waters and filtered (Whatman GF/F, 47 mm diameter, 0.7 μm pore size) to determine the total suspended material concentrations (TSM, in mg l^{-1}). Two replicas were systematically made to estimate the TSM uncertainty (5%) and the obtained TSM range was 3–300 mg l^{-1}.

Field optical measurements were carried out using a Trios-RAMSES multispectral radiometer. This sensor measures the radiance signal in the visible and near-infrared (350–950 nm) with a field-of-view of 7° and a spectral accuracy of 3.3 nm. In each station, the upwelling radiance signal was successively measured below the water surface at depths ranging from 0.02 to 0.80 m and then above the water surface. The sky radiance (L_{sky}) was measured just before and after the upwelling radiance measurements. The time between the first and last measurements was about 2 min, and so changes in the water-leaving radiance were considered insignificant. Two above-water viewing positions were systematically considered: nadir viewing ($\theta_v = 0°$); oblique viewing ($\theta_v = 40°$ and $\varphi_v = 135°$) as recommended by Mobley (1999). Within the water column, the sensor pointed downwards with a low zenith angle ($0° < \theta'_v < 30°$) that was essentially controlled by the current. The corresponding notation is therefore $L_t(0°)$, $L_t(40°)$ and $L_u(z)$ respectively. The sky radiance (L_{sky}) was successively measured with the sensor pointed towards the zenith ($\theta_v = 180°$) and related to $L_t(0°)$, then adopting an oblique viewing position ($\theta_v = 130°$ and $\varphi_v = 135°$) and related to $L_t(40°)$.

Table 1. Details of the data collected in the Plymouth Sound/Tamar estuary in June and August 2003.

Date	Location	Number of stations	Sky conditions
23/06/2003	Transect mouth—upstream	12	Cloudy
24/06/2003	Transect mouth—upstream	13	Clear—some cumulus
26/06/2003	Fixed station—upstream part	9	Thick covered
27/06/2003	Fixed station—upstream part	9	Clear
05/08/2003	Transect mouth—upstream	16	Partly cloudy then clear

3.2. Methods

The following method was adopted.

- The L_w signal was first determined from underwater $L_u(z)$ measurements.
- The L_w signal was subtracted from the total signals measured above the water.
- The respective contributions of the surface reflection effects and water-leaving signal to the total signal measured above the water were analysed.

From the recorded $L_u(z)$ measurements, previously corrected for immersion factors (Ohde and Siegel 2003), the $L_u(0^-)$ signal was determined according to equation (4). In all stations, the exponential decrease of L_u with increasing depth was clearly identified ($R^2 > 0.99$) (figure 1). The L_w signal was then estimated according to equation (5).

This L_w signal was subtracted from the total upwelling radiance signal measured above the water (L_t), then the obtained difference is the radiance signal due to surface reflection effects (cf equation (2)):

$$L_t - L_w \approx L_r. \tag{7}$$

Equation (7) was applied to the $L_t(0°)$ and $L_t(40°)$ measured signals which assumes that L_w, determined from $L_u(z)$ measurements recorded with viewing zenith angles (θ'_v) in the range 0°–30°, can be directly compared to above-water upwelling radiance signals corresponding to viewing angles (θ_v) of 0° and 40°.

From our field measurements, it is therefore possible to quantify the respective contributions of surface reflection effects and water-leaving radiance as a function of the selected viewing positions, and observe the influence of the illumination conditions and water turbidity.

4. Results

4.1. Contribution of surface reflection effects

As a proportion of the measurements were carried out under covered skies, the daily variations of L_w, $L_t(0°)$ and $L_t(40°)$ are presented as a function of time (GMT) rather than solar zenith angle.

On 24/06/2003 (clear sky), TSM concentrations increase from 08:50 to 13:53, then decrease up to 16:43. The influence of TSM variations is directly observed on L_w measured at 550, 650 and 850 nm (figure 2). It is also generally observed for the $L_t(0°)$ and $L_t(40°)$, but these signals also present significant variations not dependent on the water turbidity (induced by surface reflection effects). $L_t(40°)$ is typically higher than $L_t(0°)$ and more sensitive. At 450 and 850 nm, L_w represents less than 50% of the above-water signals, but this L_w contribution is significantly greater at 550 and 650 nm (around 80%).

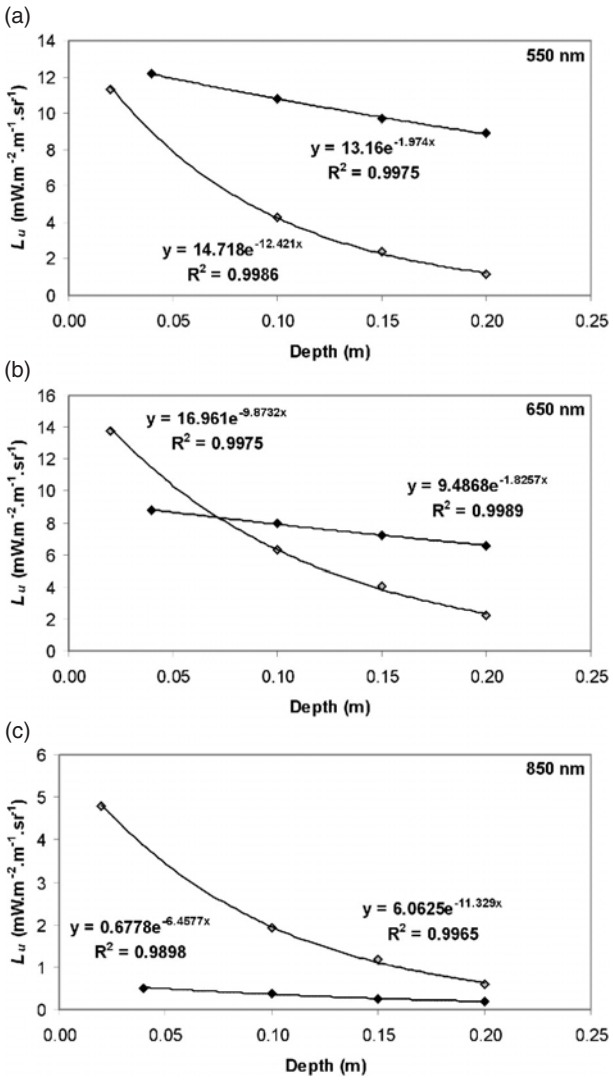

Figure 1. Extrapolation towards the surface of L_u measurements carried out at different depths. The equations of the observed exponential laws can be used to determine the L_u signal just beneath the surface. In this example, three wavelengths are selected: (a) 550 nm, (b) 650 nm and (c) 850 nm. Samples were collected on 24/06/2003 near the mouth of the Tamar estuary (TSM = 13 mg l^{-1}) (black points) and on 25/06/2003 in the upstream part of the estuary (TSM = 107 mg l^{-1}) (grey points).

Similar variations and respective contributions of L_w are observed under clear sky conditions on 27/06/2003 and 05/08/2003 (not presented). On 23/06/2003 (cloudy sky), changing illumination conditions induced a high variability of the $L_t(0°)$ and $L_t(40°)$ signals (not presented).

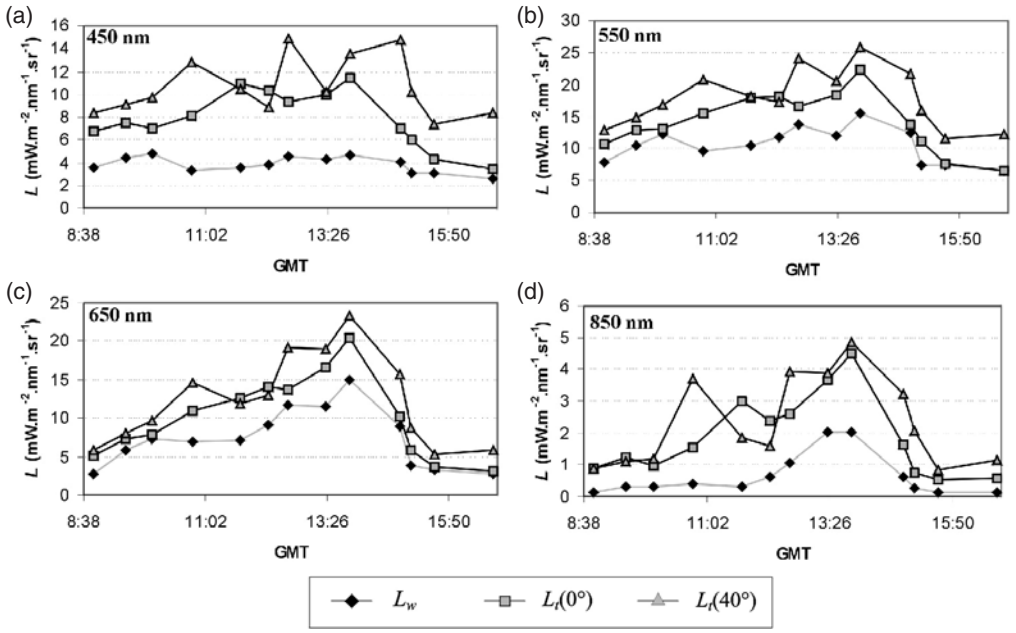

Figure 2. Comparison of the upwelling radiance signals measured above the water, $L_t(0°)$ and $L_t(40°)$, and water-leaving radiance signal (L_w) at (a) 450 nm, (b) 550 nm, (c) 650 nm and (d) 850 nm. Measurements were carried out on 24/06/2003, under a clear sky, in the Tamar estuary. The corresponding TSM concentrations increase from 7 mg l^{-1} (at 08:50) to 45 mg l^{-1} (at 13:53), then decrease to 5 mg l^{-1} (at 16:43).

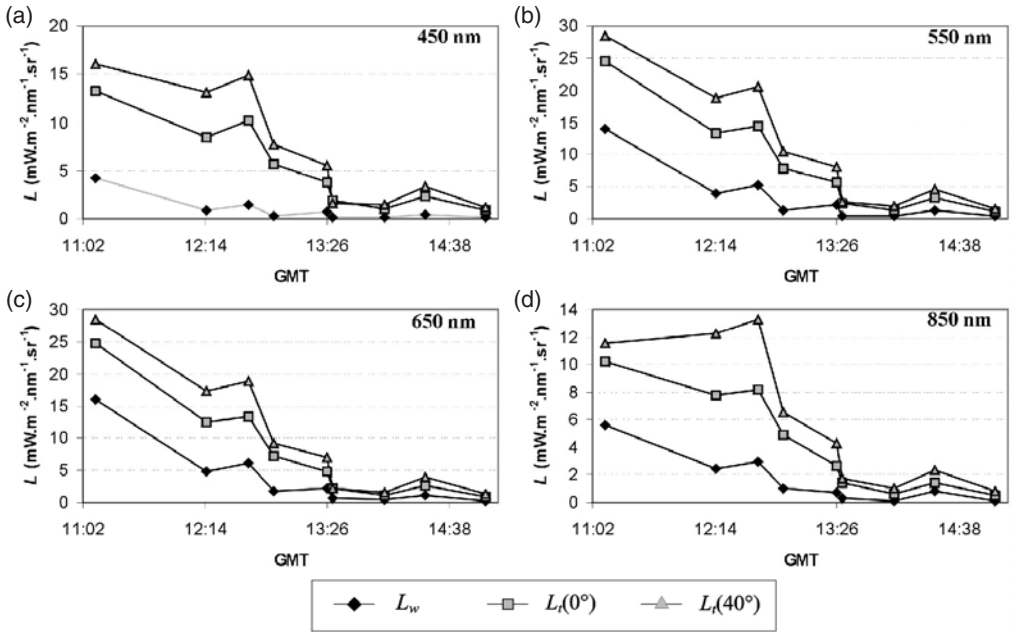

Figure 3. Comparison of the upwelling radiance signals measured above the water, $L_t(0°)$ and $L_t(40°)$, and water-leaving radiance signal (L_w) at (a) 450 nm, (b) 550 nm, (c) 650 nm and (d) 850 nm. Measurements were carried out on 26/06/2003, under a covered sky, in the Tamar estuary. The corresponding TSM concentrations globally decrease from 151 mg l^{-1} (at 11:10) to 44 mg l^{-1} (at 15:00).

On 26/06/2003 (covered sky), TSM concentrations globally decrease from 11:00 to 15:00. L_w, $L_t(0°)$ and $L_t(40°)$ closely follow these variations of water turbidity (figure 3). The $L_t(0°)$ and $L_t(40°)$ signals appear more stable than under clear skies, with L_w being low and representing less than 50% of the above-water signals at all wavelengths. Surface reflection effects are clearly predominant as already observed in similar environmental conditions (Doxaran *et al* 2003). Once again, $L_t(40°)$ is systematically higher than $L_t(0°)$.

From these observations, surface reflection effects are therefore dependant on the illumination conditions (cloud cover, solar zenith angle). Their contribution to above-water upwelling radiance measurements becomes predominant under a diffuse incident light.

Concerning viewing position, the selection of a nadir or oblique viewing position does not seem to significantly influence the quality of the above-water measurements. Contrary to recommendations (Mobley 1999, Fougnie *et al* 1999), the use

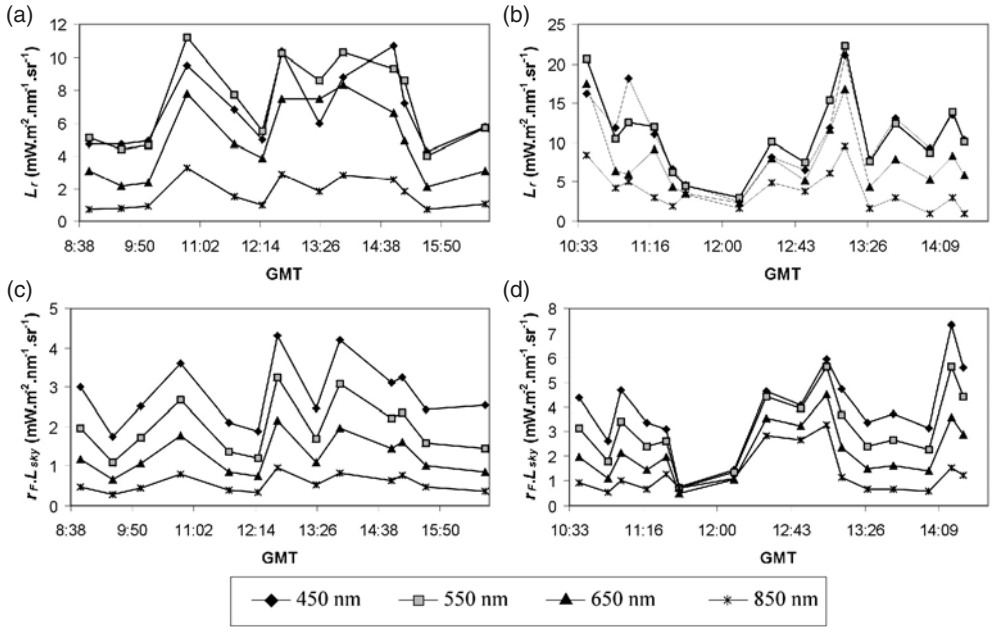

Figure 4. Plot of L_r determined according to equation (7) from measurements carried out under clear skies on (a) 24/06/2003 and (b) 05/08/2003. Comparison with the product $r_F \cdot L_{sky}$ determined on (c) 24/06/2003 and (d) 05/08/2003.

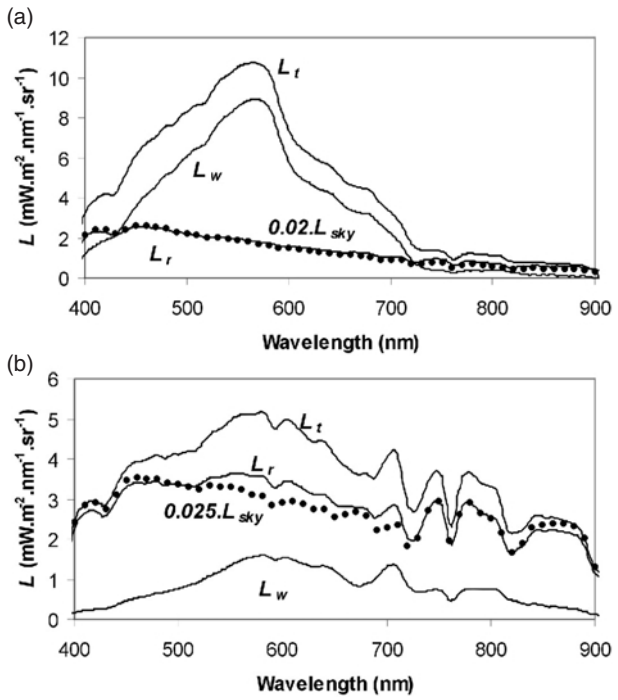

Figure 5. Examples of measured L_t and L_w radiance signals. (a) Under a clear sky (05/08/2003, 14:04 GMT) in the Plymouth Sound (TSM = 4 mg l^{-1}). (b) Under a covered sky (26/06/2003, 14:24 GMT) in the Tamar estuary (TSM = 49 mg l^{-1}). Plot of the percentage of the measured sky radiance (L_{sky}) reproducing the observed L_r signal.

of a nadir viewing position appears slightly more satisfactory, as it is systematically less affected by surface reflection effects.

With increasing water turbidity, L_w (signal backscattered by the water) logically increases. Assuming that surface reflection effects are not dependent on the water turbidity, it was expected to observe a growing contribution of L_w to L_t. This assumption is not confirmed by our observations. This may result from changing optical properties (Fresnel reflection coefficient, refractive index) in highly turbid waters, as observed by Haltrin (1998).

4.2. Influence of solar zenith angle

Surface reflection effects determined from our measurements ($L_r = L_t - L_w$) are now considered. The 24/06/2003 and 05/05/2003 data sets are selected, as representative of clear sky conditions.

According to equation (3), the obtained L_r should be identical to the measured L_{sky} multiplied by the ρ factor (actual percentage of L_{sky} reflected at the air/water interface). ρ depends on numerous parameters and an improved radiative transfer code must be used to investigate its variations (Mobley 1999). However, under optimal conditions (clear sky and plane sea surface), these variations are mainly governed by the Fresnel reflectance coefficient r_F (Austin 1974). From a latitude, longitude and time (GMT), and non-polarized light, r_F can be calculated (e.g. Bukata *et al* 1995). It increases with increasing solar zenith angle, being maximum in the early morning and late afternoon and minimum at mid-day.

In order to assess the solar zenith angle influence on our observed surface reflection effects, L_r was also determined according to the approximate formulation:

$$L_r \approx r_F \cdot L_{sky}. \tag{8}$$

Results obtained from applying equations (3) and (8) are generally similar (figure 4), but the amplitude of the obtained L_r signals is different. It indicates that the actual ρ value is systematically higher than r_F. In both cases, L_r shows large and rapid variations during the day that are not, as could be expected, governed by r_F. They essentially depend on

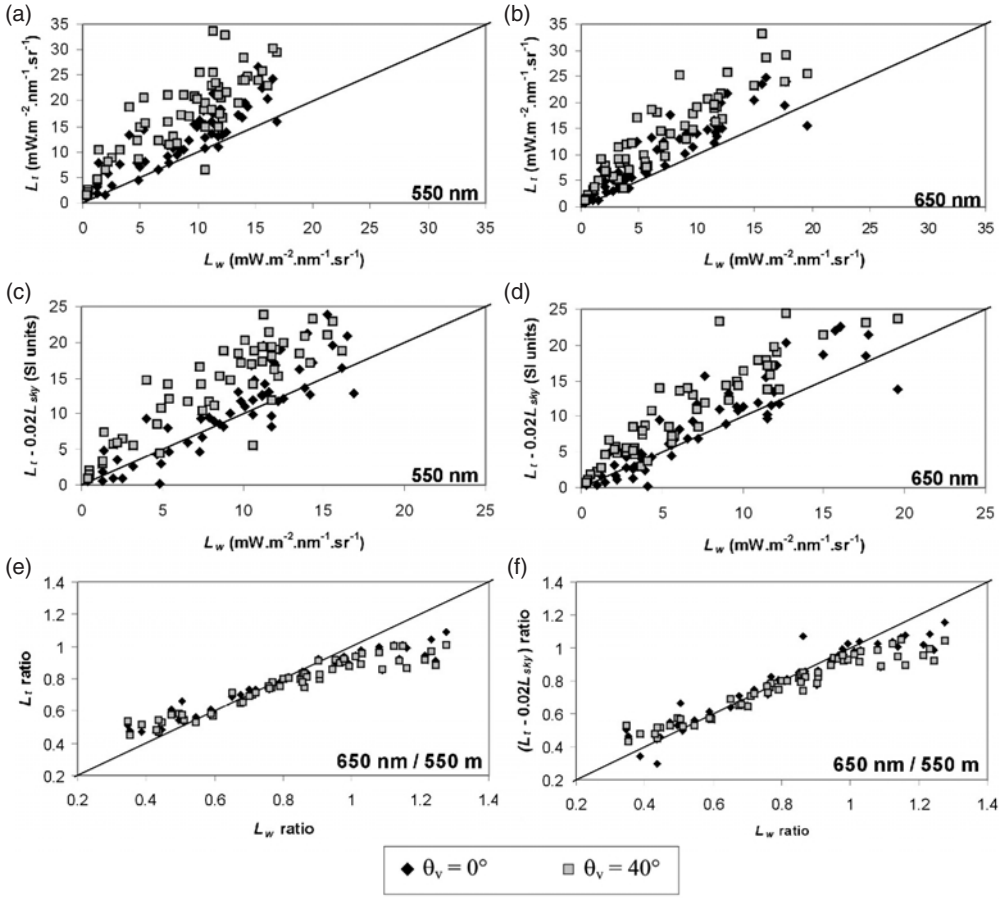

Figure 6. Plot of L_t versus L_w at (a) 550 nm and (b) 650 nm. Plot of $[L_t - 0.02L_{sky}]$ versus L_w at (c) 550 nm and (d) 650 nm. Plot of $[L_t(650\text{ nm})/L_t(550\text{ nm})]$ versus $[L_w(650\text{ nm})/L_w(550\text{ nm})]$ (e). Plot of $[(L_t - 0.02L_{sky})(650\text{ nm})/(L_t - 0.02L_{sky})(550\text{ nm})]$ versus $[L_w(650\text{ nm})/L_w(550\text{ nm})]$ (f).

L_{sky}, which appears to be a very sensitive signal influenced by the relative position of the Sun (heterogeneous skylight distribution). The high sensitivity of L_{sky} strongly influences the variations of the above-water upwelling radiance signals (see the variations of $L_t(0°)$ and $L_t(40°)$ on figure 2). Under clear skies, if the measured L_{sky} is not exactly the one reflected by the water surface (this can occur as the sea surface is not perfectly plane), large errors will be induced when applying equations (2) and (3) to above-water field measurements.

4.3. Correction of surface reflection effects

From our field measurements, the accuracy of the correction proposed in equations (2) and (3) is now analysed.

Simple cases are first considered, corresponding to optimal environmental conditions (a perfectly clear sky then covered sky, with a perfectly plane surface). Measurements carried out adopting the oblique viewing direction recommended by Mobley (1999) are considered. Hyperspectral L_t and L_w signals measured under a quasi-perfect blue sky present a very similar shape (figure 5(a)). L_t is logically higher, especially at short wavelengths (<500 nm). The observed difference, L_r, increases from near-infrared to blue wavelengths. It represents about 20% of L_t between 500 and 700 nm, and from 30% to 60% in the blue and near-infrared spectral domains. L_r is almost identical to L_{sky} multiplied by 2%, as indicated by Austin (1974) for a plane sea surface and a Sun close to the zenith. In this case, L_r can be accurately retrieved from L_t.

Under an apparently homogeneous covered sky, L_t and L_w present a very similar shape (figure 5(b)), but the magnitude of the signals is different from the clear sky case: L_r represents more than 60% of L_t between 500 and 700 nm, and up to 90% at 450 nm and in the near-infrared. It is approximately identical to L_{sky} multiplied by 2.5% (as indicated by Mobley (1999)). Once again, applying equations (3) and (4) and selecting an appropriate ρ value would give an accurate estimation of L_w.

These two examples only represent ideal cases. Most of the time, clear skies are not perfectly clear, being partly cloudy (e.g. cumulus far away from the Sun, cloud bank on the horizon), and the water surface is not perfectly plane. Cloudy and heterogeneous covered skies are also often encountered during field measurements. In these cases, it is more difficult to select an appropriate ρ value as it becomes spectral dependent and highly variable (Mobley 1999). Moreover, ρ is also influenced by the solar zenith angle and viewing position. Surface reflection effects appear to be highly significant and predominant whatever the illumination conditions (see section 4.1). Selecting an inappropriate ρ factor results in an inexact value for L_r and large errors in the retrieved L_w. These errors are analysed for the complete set of data collected in June and August 2003. L_t, uncorrected for surface reflection

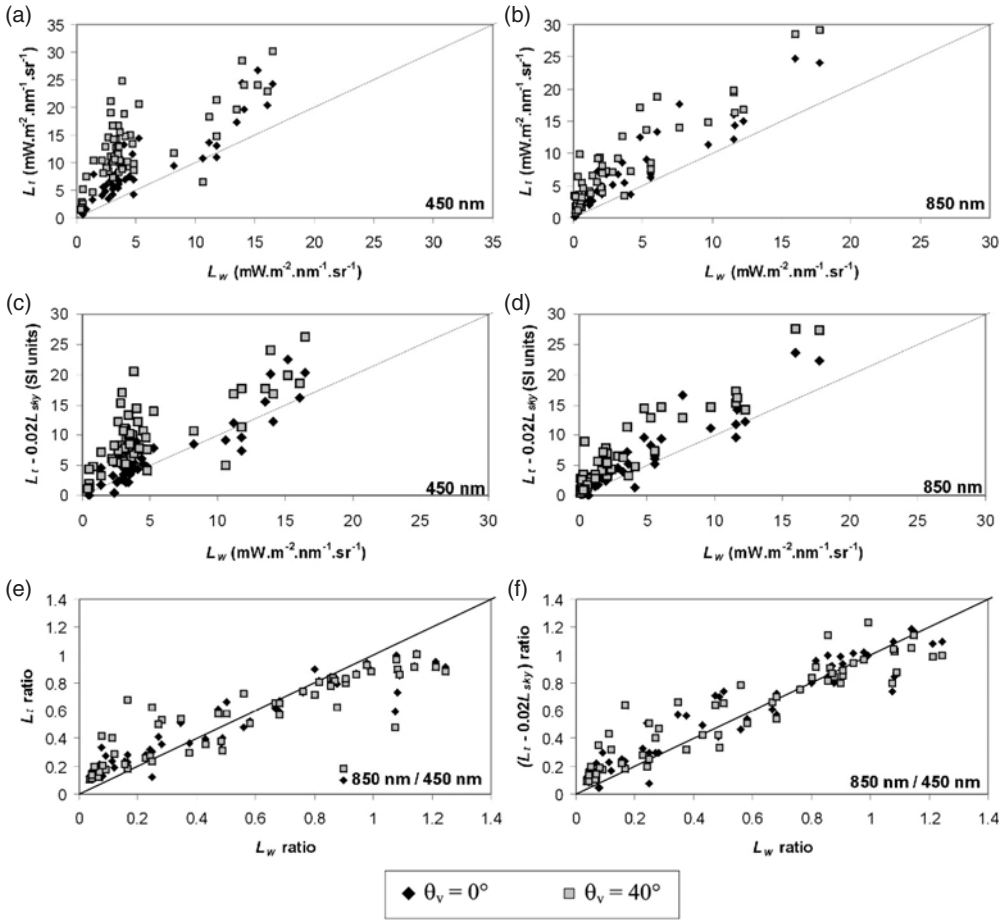

Figure 7. Plot of L_t versus L_w at (a) 450 nm and (b) 850 nm. Plot of $[L_t - 0.02L_{sky}]$ versus L_w at (c) 450 nm and (d) 850 nm. Plot of $[L_t(650\ nm)/L_t(550\ nm)]$ versus $[L_w(850\ nm)/L_w(450\ nm)]$ (e). Plot of $[(L_t - 0.02L_{sky})(850\ nm)/(L_t - 0.02L_{sky})(450\ nm)]$ versus $[L_w(850\ nm)/L_w(450\ nm)]$ (f).

effects then corrected adopting an approximate 0.02 ρ value, is compared to L_w.

The obtained results confirm the previous observations: L_t is logically higher than L_w; adopting an oblique viewing position rather than a nadir viewing position results in higher surface reflection effects (figures 6(a) and (b)). By selecting an approximate 0.02 ρ value, L_t was undercorrected for surface reflection effects, resulting in a dramatic overestimation of L_w (figures 6(c) and (d)). These results tend to discredit above-water optical measurements. However, a practical solution can be applied to minimize the errors resulting from imperfect correction of surface reflection effects. When considering a ratio between two wavelengths (here 650 and 550 nm), the contamination of the ratio by residual surface reflection effects decreases and almost disappears (figures 6(e) and (f)). Best results are obtained in the case of the $(L_t - 0.02L_{sky})$ signal (figure 6(f)), that can be written

$$L_t - 0.02L_{sky} = L_w + L_{sky\_res}, \tag{9}$$

where L_{sky_res} is the radiance signal resulting from residual surface reflection effects after an approximate correction. L_{sky_res} is typically low compared to L_w and its influence is therefore reduced when considering a ratio between two wavelengths. These observations are confirmed when regarding the root-mean-square differences between the measured L_t then $(L_t - 0.02L_{sky})$ signals and L_w, noted respectively rmsd and rmsd_{sky} (table 2).

Similar results are obtained at 450 and 850 nm (see figure 7 and table 2). At 450 nm, L_t is essentially dependent on surface reflection effects, notably when L_w is low (i.e. low water turbidity) (figure 7(a)). At 850 nm, L_t increases almost linearly with L_w but is also highly influenced by surface reflection (figure 7(b)). The applied approximate correction (equation (9)) is not satisfactory, and the resulting obtained L_w were overestimated at 450 and 850 nm (figures 7(c) and (d); table 2). When considering a ratio between these two wavelengths, results are significantly improved and the corresponding L_w ratio is reasonably estimated (figures 7(e) and (f)). Thus, even when considering two wavelengths predominantly affected by surface reflection effects, the ratio approach significantly reduces the contamination.

5. Conclusions

Based on field optical data recorded in turbid coastal and estuarine waters, the respective contributions of water-leaving radiance and surface reflection effects to above-water upwelling radiance measurements have been estimated. Two different viewing directions (vertical and oblique) were considered; different illumination conditions (cloud cover, solar zenith angle) were encountered.

Table 2. Root-mean-square differences (rmsd and rmsd_{sky}) between the measured above-water upwelling radiance signals (L_t and $[L_t - 0.02L_{\text{sky}}]$, respectively), and L_w at (a) selected wavelengths, (b) selected wavelength ratios. The two viewing directions ($\theta_v = 0°$ and 40°) are considered.

(a)	rmsd (mW m^{-2} nm^{-1} sr^{-1})		rmsd_{sky} (mW m^{-2} nm^{-1} sr^{-1})	
Wavelength (nm)	$\theta_v = 0°$	$\theta_v = 40°$	$\theta_v = 0°$	$\theta_v = 40°$
450	4.90	9.38	2.70	6.36
550	5.00	9.82	3.28	7.38
650	4.09	7.52	2.85	5.72
850	3.19	5.40	2.28	4.17
(b)	rmsd (dimensionless)		rmsd_{sky} (dimensionless)	
Wavelength ratio	$\theta_v = 0°$	$\theta_v = 40°$	$\theta_v = 0°$	$\theta_v = 40°$
650 nm/550 nm	0.10	0.12	0.12	0.11
850 nm/450 nm	0.19	0.24	0.27	0.22

The contribution of surface reflection effects appeared highly variable and always significant whatever the illumination conditions. Under a clear sky, they represent about 50% of the total above-water signal between 500 and 700 nm, and more than 50% at short (<500 nm) and near-infrared wavelengths. They become predominant (typically 80%) under a diffuse incident light. The measured sky radiance appeared to be highly sensitive, especially under clear skies, resulting in highly variable above-water upwelling radiance. This variability was observed independently of the viewing position (nadir or oblique).

A limited influence of surface reflection effects was expected in highly turbid waters, where the water-leaving signal is high, but this assumption was not confirmed from our measurements. This may result from changing optical properties (e.g. Fresnel reflection coefficient) with increasing suspended solid concentration (Haltrin 1998).

The correction of surface reflection effects recommended by Mobley (1999) (subtraction of the percentage, ρ, of the sky radiance reflected at the air/water interface) was applied to field data. Results were not satisfactory due to the difficulty in selecting an appropriate ρ value (amplitude and spectral variations). Selecting an approximate ρ value of 2% resulted in a significant overestimation of the retrieved L_w. However, the error was considerably reduced when a ratio between two wavelengths was considered.

Further measurements (using at least two spectroradiometers) and numerical computations (using radiative transfer codes) are needed to improve the understanding of reflection phenomena at the air/water interface.

Acknowledgments

This work was supported by a European Marie Curie fellowship (Framework 5, EVK3-CT-2002-50012) and NERC small grant (NER/B/S/2002/00555, PI Lavender).

References

Austin R W 1974 Inherent spectral radiance signatures of the ocean surface *In Ocean Color Analysis* (La Jolla, CA: Scripps Inst. Oceanogr.) p 195

Austin R W 1980 Gulf of Mexico, ocean-colour surface-truth measurements *Bound.-Layer Meteorol.* **18** 269–85

Bukata R P, Jerome J H, Kondratyev A S and Pozdnyakov D V 1995 *Optical Properties and Remote Sensing of Inland and Coastal Waters* (Boca Raton, FL: CRC Press) p 71

Doxaran D, Froidefond J M and Castaing P 2002a A reflectance band ratio used to estimate suspended matter concentrations in sediment-dominated coastal waters *Int. J. Remote Sens.* **23** 5079–85

Doxaran D, Froidefond J M, Lavender S J and Castaing P 2002b Spectral signature of highly turbid waters. Application with SPOT data to quantify suspended particulate matter concentrations *Remote Sens. Environ.* **81** 149–61

Doxaran D, Froidefond J M and Castaing P 2003 Remote sensing reflectance of turbid sediment-dominated waters. Reduction of sediment type variations and changing illumination conditions effects using reflectance ratios *Appl. Opt.* **42** 2623–34

Fargion G S and Mueller J L 2000 Ocean optics protocols for satellite ocean color sensor validation, Revision 2, *NASA Technical Memorandum 209966* (*SeaWiFS Technical Report Series*) (Greenbelt, MD: NASA Goddard Space Flight Center)

Fougnie B, Frouin R, Lecomte P and Deschamps P Y 1999 Reduction of skylight reflection effects in the above-water measurements of diffuse marine reflectance *Appl. Opt.* **38** 3844–56

Froidefond J M, Castaing P, Mirmand M and Ruch P 1991 Analysis of the turbid plume of the Gironde (France) based on SPOT radiometric data *Remote Sens. Environ.* **36** 149–63

Froidefond J M, Castaing P and Prud'homme R 1999 Monitoring suspended particulate matter fluxes and patterns with the AVHRR/NOAA-11 satellite: application to the Bay of Biscay *Deep-Sea Res.* II **46** 2029–55

Haltrin V I 1998 Fresnel reflection coefficient of very turbid waters *Proc. 5th Int. Conf. on Remote Sensing for Marine and Coastal Environments (Ann Arbor, MI)* vol 2, pp 361–7

Mobley C D 1994 *Light and Water: Radiative Transfer in Natural Waters* (San Diego, CA: Academic) p 592

Mobley C D 1999 Estimation of the remote-sensing reflectance from above-surface measurements *Appl. Opt.* **38** 7442–55

Morel A 1980 In-water and remote sensing measurements of ocean color *Bound.-Layer Meteorol.* **18** 177–201

Morel A and Gentili B 1996 Diffuse reflectance of oceanic waters. II. Implication of bidirectionality for the remote-sensing problem *Appl. Opt.* **35** 4850–61

Ohde T and Siegel H 2003 Derivation of immersion factors for the hyperspectral TriOS radiance sensor *J. Opt. A: Pure Appl. Opt.* **5** 12–4